Subduction initiation at the Soloman back-arc basin: Contributions from both island arc rheological strength and oceanic plateau collision

Liangliang Wang[1,2], Liming Dai[1,2*], Wei Gong[1,2], Sanzhong Li[1,2*], Xiaodian Jiang[1,2], Gillian Foulger[3], Hao Dong[1,2], Zhonghai Li[4] & Shengyao Yu[1,2]

[1] Key Lab of Submarine Geosciences and Prospecting Techniques, Frontiers Science Center for Deep Ocean Multispheres and Earth System,MOE and College of Marine Geosciences, Ocean University of China, Qingdao 266100, China

[2] Laboratory for Marine Mineral Resources, Qingdao National Laboratory for Marine Science and Technology, Qingdao 266100, China

[3] Department of Earth Sciences, Durham University, Science Laboratories, South Rd. DH1 3LE, UK

[4] Key Laboratory of Computational Geodynamics, College of Earth and Planetary Sciences, University of Chinese Academy of Sciences, Beijing, China

Corresponding author: Liming Dai (dlming@ouc.edu.cn) & Sanzhong Li (sanzhong@ouc.edu.cn)

Key Points:

- The subduction initiation at the SSB results from a joint contributions of both SIA rheological strength and OJP collision;
- The island arc affects the development of shear zone between an island arc and back-arc basin which favors subduction initiation;
- The mass depletion of lithospheric mantle in the OJP influences evolution of subduction patterns after subduction initiation.
-

Abstract

It is generally accepted that the subduction polarity reversal (SPR) results from the strong collision of two plates. Yet, the SPR of the Solomon Back-arc Basin is started in the “soft docking” stage and the mechanism by which the ”soft docking” induced subduction initiation (SI) remains elusive. We find that the mass depletion of the plateau influences the evolution of the subduction patterns during SI. And the island arc rheological strength affects the development of the shear zone between an island arc and back-arc basin which favors SI. What’s more, with the increase of the rheological strength difference, the SI is more easily to occur, and the contribution of the plateau collision to SI weakens. Hence, by combining the available geological evidence, we suggest that the Solomon Island Arc rheological strength and the Ontong-Java plateau collision jointly controlled the SI during the ”soft docking” stage.

Plain Language Summary

Plateau collision has been considered as an important factor for the subduction initiation (SI). However, the SI of the Solomon Sea Basin occurred during the "soft docking" stage, which is unique from the traditional understanding of SI. Our numerical model shows that the rheological strength difference between the SIA and the Solomon Sea basin results in the conjugate shear zone with high strain rate during the "soft docking" stage. The conjugate shear zone with high strain rate as a natural weak zone is conducive to inducing SI. Moreover, while the SI (the San Cristobal Trench) occurs, the OJP likes a "wall" has resulted in the uplift of the SIA and the distinct evolution of subduction patterns.

1 Introduction

Subduction initiation (SI) is key to study the evolution of the solid Earth and has profound implications for plate motion (Arculus et al., 2015; Crameri et al., 2020; Gerya et al., 2015; Lallemand & Arcay, 2021; Maunder et al., 2020; Niu, 2016; Stern & Gerya, 2018; Sutherland et al., 2020). Recent researches proposes that there are two types of subduction initiation: vertically-forced and horizontally-forced SI (Crameri et al., 2020; Lallemand & Arcay, 2021). Vertically-driven SI is purely driven by gravity- or density-induced buoyancy, whilst horizontally-driven SI is attributed to laterally-driving forces that arise, for example, from tectonic- or mantle-convection induced stresses (Bhattacharya et al., 2019; Crameri et al., 2020; Crameri & Tackley, 2014, 2015; Duretz et al., 2016; Faccenda et al., 2008; Guilmette et al., 2018; Van Hinsbergen et al., 2015; Maffione et al., 2015, 2017; Maunder et al., 2020; Plunder et al., 2020; Stern, 2004; Tetreault & Buiter, 2012; Vogt & Gerya, 2014; Zhou et al., 2020). Subduction polarity reversal (SPR), a type of horizontally-forced SI, seems to be one of the more common SI mechanisms throughout the last 100 Myr (Almeida et al., 2022; Crameri et al., 2020; Zhang & Leng, 2021), e.g., in the Andaman Islands arc (Plunder et al., 2020), beneath Taiwan (von Hagke et al., 2016; Tao et al., 2020), and the Aleutian Arc (Vaes et al., 2019), the New Hebrides (Falvey & D., 1975), and the Solomon Island Arc (SIA) (Mann & Taira, 2004). A typical SPR example is the San Cristobal Trench along the SIA, which may have resulted from the convergence of Ontong-Java plateau (OJP) and the SIA (Holm et al., 2016; Mann & Taira, 2004; Petterson et al., 1999; Stern, 2004; Tapster et al., 2014).

The OJP, as the most extensive large igneous province (Mann & Taira, 2004), may be created by the cataclysmic outpouring of magma from the mantle plume head, or may result from eclogite upwelling in a ridge (Korenaga, 2005). Although the exact nature of the OJP origin remains elusive, the widespread emplacement of the OJP began at ~122 Ma in the southern Pacific Ocean (Chandler et al., 2012). Once formed, the OJP drifted northward with the rest of the Pacific Plate (Figure 1a) (Knesel et al., 2008). The initial arrival of the OJP at the North Soloman Trench (NST) at ~22 Ma (Early Miocene) was termed a "soft docking" event which is typically characterized by the absence of the significant deformation in the SIA and OJP (Figure 1b) (Petterson et al., 1999). In addition, according to the pre-existing plate reconstruction (Müller et al., 2019), the

OJP and the SIA at this time converged obliquely and the velocity component of the OJP moving towards the SIA was very low, near 0 cm/yr, while the Australian Plate continued to move northward with a velocity component of about 3 cm/yr (Figure 1b). In this "soft docking" tectonic setting, the age of the SPR in this subduction system has been proposed to fall between 14 and 8 Ma, is prior to the "hard docking" stage occurred at 6 Ma which is typically characterized by strong deformation of the SIA (Figure 1c) (Hall, 2002; Schellart et al., 2006; Austermann et al., 2011; Petterson et al., 1999). However, the SPR along the southern flank of the SIA is started in the "soft docking" stage, which is unique from the traditional understanding of SPR results from the strong collision of two plates (Almeida et al., 2022; Hall, 2002; Lallemand & Arcay, 2021b; Stern & Gerya, 2018; Sun et al., 2022; Taira et al., 2004). Consequently, questions concerning why the "soft docking" can induce SI still await answer

To understand why the SI started in the "soft docking" stage, here thermomechanical modeling is employed. A series of numerical modeling experiments (Figure S1) are carried out to gain new insights on the SI during the "soft docking" stage. The model includes the initial OJP mantle depletion, variations in the compositional mantle buoyancy (Mann & Taira, 2004; Tharimena et al., 2016), and melts from the oceanic crust, sediments and the OJP's crust. With this model, we are able to demonstrate how subduction initiation can be triggered by the interaction between an island arc and a large-scale oceanic plateau with a depleted lithospheric mantle.

2 Model geometry and initial boundary conditions

Our two-dimensional magmatic thermodynamic model simulates collision between the OJP and the SIA which led to the initiation of subduction in the back-arc basin. The governing equations of conservation of momentum, mass and energy are solved with the I2VIS code (Gerya & Yuen, 2003).

We conducted a series of numerical experiments with various oceanic plateau lengths and properties, island arc lengths and thicknesses, and lithospheric thickness of the back-arc basin.

The numerical models include two domains: the left-side arc/back-arc and the right-side oceanic plateau. The transition between these two domains is separated by a weak zone. Previous studies suggest that the OJP is much thicker than most of oceanic plateaus and is 33 km thickness on average (Liu et al., 2021; Mann & Taira, 2004). We determine the density of the plateau, and the density of its each layer, from the P-wave velocity structure, and then further constrain the correctness of the model using Crust1.0 (Laske et al., 2013). A thin "sticky air" layer with low density and viscosity is also applied (Crameri et al., 2012), which allows the direct calculation of topographic evolution. An asthenospheric mantle is imposed below the continental and oceanic lithosphere.

The oceanic plateau is 1120 km wide and has a 26.6-km-thick oceanic crust underlain by a reworked lithospheric mantle. The oceanic plate on which the OJP resides has a normal oceanic plate thickness of 8 km (Figure S1). The

plateau is set as a trapezoid because the thickness of the plateau decreases from the inside to the outside (Figure S1). Based on seismic wave speed data and Crust1.0 model, we infer that the OJP crust is divided into three layers. The oceanic plateau crust is 26.6 km thick and consists of an upper crust (a 2.66-km-thick layer of basaltic rock), a middle crust (a 5.3-km-thick layer of gabbro) and an 18.64-km-thick layer of ductile ultramafic rock (Figure S1). Besides, more recent data suggest that the OJP has a thick viscous mantle root (Isse et al., 2021; Tharimena et al., 2016). Seismic and geochemical constraints reveal that the lithospheric mantle beneath the oceanic plateau may also be stratified into two layers, comprising typical oceanic lithosphere (with a thickness of 44 km) underlain by a layer that includes a lithosphere mantle enriched in refractory harzburgites (with a thickness of 45 km) (Covellone et al., 2015; Ishikawa et al., 2004, 2011; Isse et al., 2021; Mann & Taira, 2004; Tharimena et al., 2016). Since the OJP is not completely subducted, we consider that the length and the mantle viscosity of the oceanic plateau have a minor impact on the SI during collision. But the mass depletion lithospheric mantle of the oceanic platea is an important parameter that we took into account. And, the material properties and parameters in this study are shown in Table. S1&2.

According to the Crust1.0 model and recent crustal velocity model (Holm et al., 2019; Ku et al., 2020), the arc crustal thickness in our models is asymmetric. The left part has a thickness of 28 km and the right part is a thickness of 34 km. Previous studies suggest that the SIA is an island arc with an affinity of continental crust (Tapster et al., 2014). So we set up the SIA with continental crust properties in our model. The arc is composed of two layers: the felsic upper crust with the thickness of 17 km and 20 km at the left and right sides, respectively, and with rheological properties of wet quartzite; and the mafic lower crust with the thicknesses of 11 km and 14 km at the left and right sides, respectively, and with the rheological properties of plagioclase. Apart from that, the length of the current Solomon Arc in our reference model is about 340 km, depending on the island arc under compression being about 250 km length in the present-day state (Figure 1c orange line) (Müller et al., 2019).

The initial temperature structure of the model varies from 0°C at the surface to 1300°C at the bottom of the lithospheric mantle(Shi et al., 2020). The initial temperature gradient of the asthenospheric mantle is ~0.5°C/km(Shi et al., 2020). The detailed compositions and temperature profile of our models are shown in Figure S1. The rock properties and layer thicknesses depend on the model parameters (Table S1).

The thermal structure of the oceanic lithosphere was calculated from the half space cooling model (Turcotte & Schubert, 2002) for a given plate age of 100 Ma. The ages of the oceanic part of the Australian Plate lie between 49 Ma and 25 Ma, based on plate tectonic reconstruction (Hall, 2002) and the recent regional studies (Müller et al., 2019).Thus, the initial thermal structure of the back-arc is defined with a plate lithospheric depth of 88 km and the age is taken to be 30 Ma. Our model is similar to a previous numerical modelling study that investigated

variations in oceanic–continental and intra-oceanic subduction modes (Dai et al., 2020; Z. H. Li et al., 2019; Tao et al., 2020; Zhou et al., 2018, 2020).

We apply free slip motion at all boundaries except for the lower boundary that is permeable (Z. H. Li et al., 2019). In addition, both the subducting and overriding plates are pushed internally by constant convergence velocities in the yellow squares as shown in Figure S1, which produces approximately uniform velocity of the horizontally moving plates. The oceanic plate moves to the right side of the model with a prescribed convergent rate Vx (Figure S1).

3 Results

With the regional-scale two-dimensional (2D) models, we investigate the dynamic evolution of subduction initiation in the presence of the OJP (Figure S1, Methods). The initial stage of the reference model is subduction of the Pacific Plate beneath the SIA. The SI begins during "soft docking" when the oceanic plateau just reaches the trench and the intersection area between the island arc and back-arc basin shows an obvious strain rate drop (Figures 2&4; see Discussion). During the "soft docking" stage, no obvious deformation can be found in the island arc as previous results (Figure 2g) (Mann & Taira, 2004; Petterson et al., 1999). With the ongoing plate convergence, the new subduction zone under advancing subduction pushed the island arc to collide strongly with the OJP, this subduction stage corresponds to the "hard docking" stage. This process resulted in a strong deformation of the island arc to form two anticlines and one syncline, further led to the passive accretion of the upper part of the oceanic plateau, and resulting in the strain rate increases in the intersection area (Figure 2h; see Discussion). During this time, the topography of the island arc transforms from single-peaked to double-peaked in shape (Figures 2e). And then, under continuous advancing subduction, the new slab interacts with the old to result in the slab detachment of the old slab (Figure 2a).

In addition, we have run almost 560 model cases in total (Table S2 in supporting information) and found three key regions to control the SPR according to the statistical results (Figure S2). They are the oceanic plateau with data of its lithospheric mantle density; and the island arc with data of its crust thickness, length; and the back-arc basin with its lithospheric thickness. Our simulations adopt four different lithospheric responses is shown in Figure S2-S4 & Supplementary Information: (1) a single subduction model (SSM); (2) a double subduction model (DSM); (3) a mantle detachment model (MDM); and (4) fracturing of the back-arc basin model (FBM).

4 Discussion

4.1 Model results versus natural data

While a subducting slab along the pre-existing subduction zone already stagnated (Mann & Taira, 2004), some seismic activities still appear in this region (Figure S5a). The reference model indicates that the occurrence of these seismic events may be due to passive subduction of the OJP, caused by obduction of

the island arc (Figure 2). In addition, the new subducting slab collided with the old slab at a depth of 350 km during the persisted subduction, resulting in a detachment of the old slab to form mantle micro-blocks which can be imaged in high-resolution seismic tomography (Figure S5b) (Li et al., 2018).

Furthermore, our reference model matches well with recent terrain and structural model (Figure 2) (Mann & Taira, 2004). During the "hard docking" stage, due to a compression along the new subduction zone and an obstruction of the oceanic plateau, the SIA experienced multiple-stage deformation (Mann & Taira, 2004; Petterson et al., 1999) that ultimately resulted in a region with bimodal topography which is constant with the terrain statistics in this region (Figures 2b,d). Our model shows that the lithospheric mantle beneath the island arc can thrust partially over the OJP, which may correspond to the high-velocity anomaly in Figure 2c (Mann & Taira, 2004).

4.2 Role of the slab break-off in subduction initiation

In addition to the jamming effect of the buoyant plateau obstruction, the slab break-off is thought to be another mechanism for SI (Almeida et al., 2022; Baes et al., 2011; Sun et al., 2021). The slab break-off will induce mantle flow, causing the back-arc lithosphere to rupture and be dragged down into the mantle wedge (Baes et al., 2011; Zhang & Leng, 2021). Our results find that if the old slab has been broken-off, it can induce mantle flow to weaken the overlying plate (Figure S6). However, the weakening is not sufficient to cause lithospheric break-up and onset of subduction in the youngest Solomon Sea basin (about 40-25 Ma) with a lower lithospheric density (Maunder et al., 2020; Zhang & Leng, 2021; Zhou & Wada, 2021). And, it is worth noting that the SI in our reference model is preceded to slab detachment caused by newly subducting slab (Figure 2) rather than the old slab break-off. Therefore we consider that slab break-off is not able to initialize new subduction in study area (Figure S6)

4.3 Role of the Ontong-Java Plateau in subduction initiation

In order to identify the role of the OJP in the subduction initiation, we altered lithospheric mantle density of the oceanic plateau in our model. The mass depletion lithospheric mantle of the OJP, which is confirmed by geophysical observations (Ishikawa et al., 2011; Smart et al., 2019), may play a major role. However, the possibility that the OJP lithospheric mantle conditions inform the subduction process has not yet been explored. In order to quantify the effect of OJP lithospheric mantle density on the subduction process, we used P-wave velocity and Crust1.0 models to determine the density and the structure of the oceanic plateau crust (see Methods) (Laske et al., 2013; Mann & Taira, 2004). Based on these constraints, we use our model to explore how various degrees of lithospheric mantle depletion affect subduction initiation.

According to the theory of isostacy, a deficit of lithospheric material will lead to uplift of the terrain. Figure 3 shows the conditions that favor development of a double subduction zone. The amount of mass depletion present in each model is shown in Figure 3b, and the corresponding average topography uplift

is indicated by color. According to the subduction behavior of the model, the experimental results fall into two categories (Figure 3 e-f). An example of the double subduction zone outcome is shown in Model 1 (Figure 3 a,c,e). This model shows the appearance of new subduction zones and complete preservation of the island arc mantle. An example of the mantle detachment outcome is shown in Model 2 (Figure 3 a,d,f), in which subduction still occurs despite complete detachment of the island arc lithospheric mantle.

Our model results show that in the "soft docking" stage (Mann & Taira, 2004; Petterson et al., 1999), the dynamic behavior of the two models is similar. In both cases, a new subduction zone develops in the high-conjugate shear-strain-rate zone at the junction of the island arc and the back-arc basin (Figures 3c,3e). Due to the degree of lithospheric mantle depletion beneath the plateau, the two modes differ in their dynamic behavior during SI. In the double subduction model (Model 1), the topography of the oceanic plateau is greatly uplifted due to the large depletion of lithospheric mantle. the oceanic plateau, the topography of which is uplifted greatly, blocks obduction of the island arc and uplifts the island arc. With continuous convergence, the oceanic plateau, which is difficult to subduct, makes the island arc uplift, leading to development of a conjugate high-shear-strain-rate zone inclined to the oceanic plateau (Figures 3c,3e inset diagram). The accumulated stress can thus only be released through new subduction, giving rise to the double subduction model (Figures 3c,e).

As the degree of mantle depletion decreases, the double subduction model gradually transits to the mantle detachment model (Figures 3d,3f). In the transition region, double subduction and lithospheric mantle detachment are not completely distinguishable. As the mass depletion continuously increases, the lithospheric mantle detachment is completely dominant. The decrease of mass depletion reduces uplift of the oceanic plateau topography, leading to a weak blocking of the oceanic plateau to obduction of the island arc. Then, the island arc can rise more quickly, inducing the partial oceanic plateau being passively subducted. Thus, the high conjugate shear strain rate zone inclined toward the ocean basin develops more easily. Lithospheric mantle detachment occurs once the island arc crust and the lithospheric mantle are decoupled, leading to rapid motion toward the right of the newly trench.

One interesting finding is that the conjugate shear zone with high strain rate, as a natural weak zone, facilitates subduction initiation (Figure 3). In the "soft docking" stage (Petterson et al., 1999), the development direction of the conjugate shear zone with high strain rate is different (i.e. the double subduction model and the lithospheric mantle detachment model) as a result of the mantle with mass depletion beneath the oceanic plateau. The location of the conjugate shear zone with high strain rate, which appears in the transition region between the island arc and the back-arc basin, is mainly controlled by variations in the structural and rheological properties in these two areas.

4.4 Role of the SIA and Soloman Back-arc Basin in subduction initiation

The analysis of the average strain rate calculated for the intersection area between the island arc and back-arc basin reveals that the SI and the oceanic plateau collision with time interval (Figure 4a). We find that the intersection area has an obvious phase of strain rate drop during the "soft docking" stage (Figure 4a), which corresponds to the process of SI. When the new subduction zone has initiated, the strain rate in the intersection area increases, leading to a strong deformation of the island arc and a rapid accretion of the oceanic plateau during the "hard docking" stage (Figure 2 and 4a). Moreover, the time interval of the strain rate drop is negatively correlated with the thickness of the island arc (Figure 4a inset diagram). As the thickness of the island arc increases, the rheological strength difference between island arc and back-arc basin gradually increases (Huangfu et al., 2018), causing the SI progressively earlier than the oceanic plateau collision, which also implies that the role of the oceanic plateau to the SI is gradually weakening. The results may provide new insights into the multi-subduction systems in Tethys, and multi-subduction zones may be controlled by the rheological strength difference (e.g. Xu et al., 2013).

The control of island arc thickness on the strength and rheology of the lithosphere can be visualized using a 1D lithospheric strength profile (Figure 4b-d). These profiles are based on the same lithological stratification of the island arc (or back-arc basin) and the same rheological properties as in the 2D simulations. In order to characterize the strength difference between island arc and back-arc basin, we used the the island arc thickness as the reference parameter. For example, with a lower lithospheric strength difference between island arc and back-arc basin (Figure 4b), the lithosphere does not rupture and maintains a stable single subduction state (Figure 4b and S7). The collison between the Magnitogorsk Arc and the Laurussia Margin in the Middle through Late Devonian may be an excellent case of the single subduction model, which only happens with accretion and no SPR (Brown et al., 2011). With a larger lithospheric strength difference (Figure 4c), the lithospheric mantle and crust of the island arc are more likely to be decoupled, resulting in a mantle detachment (Figure 4d). A well-known example of the mantle detachment model is the Ozernoy-Valagina Arc, the thickness of which is about 34-36 km (Levin et al., 2002). If the lithospheric strength difference is significant, it leads to fracture of the back-arc basin (Figure 4d). In addition, the island arc length and the lithospheric thickness of the back-arc basin have a contribution to subduction initiation as well (Figure S2 and Supplementary text 2). But, the structural properties of SIA have a certain inevitability with double subduction (Ku et al., 2020; Müller et al., 2019; Pasyanos et al., 2014).

In summary, we suggest that the Solomon Island Arc rheological strength and the OJP collision jointly controlled the SI during the "soft docking" stage. And our models reveals that the mass depletion of lithospheric mantle beneath the OJP had a greater influence on the development of the conjugate shear zone of high strain rate during SI, and then led to different evolutionary patterns– double subduction and mantle detachment. Moreover, the rheological strength difference between island arc and back-arc basin which is controlled by island arc

structure on subduction initiation cannot be ignored. The contribution of the rheological strength difference to the SI is more pronounced with the increase of the rheological strength difference. This may provide a reasonable explanation for that the subduction initiation has occurred during the "soft docking" stage when the island arc was not strongly deformed.

Acknowledgments, Samples, and Data

We thank Lucy Flesch for handling the manuscript, Fabio Crameri and another anonymous reviewer for constructive comments. The research leading to these results has received funds from NSFC projects (Grants 91958214, 91858215, 41402172, 41688103, 42121005, 42176064 and 91855208), the National Key Technologies R&D Program (2017YFC0601401; 2017YFC0601300-01; 2016YFC0601002), Taishan Scholar Program to Prof. Sanzhong Li (tspd20210305) & Yongjiang Liu, and Qingdao Leading innovation talents (19-3-2-19-zhc), the Fundamental Research Funds for the Central Universities (202161011). We thank LetPub (www.letpub.com) for linguistic assistance and pre-submission expert review. The authors declare that they have no known competing financial interests or personal relationships that could have appeared to influence the work reported in this paper. All related data are provided in Zenodo (https://doi.org/10.5281/zenodo.5839086).

References

Almeida, J., Riel, N., Rosas, F. M., Duarte, J. C., & Schellart, W. P. (2022). Polarity-reversal subduction zone initiation triggered by buoyant plateau obstruction. *Earth and Planetary Science Letters*, *577*, 117195. https://doi.org/10.1016/J.EPSL.2021.117195Arculus, R. J., Ishizuka, O., Bogus, K. A., Gurnis, M., Hickey-Vargas, R., Aljahdali, M. H., et al. (2015). A record of spontaneous subduction initiation in the Izu-Bonin-Mariana arc. *Nature Geoscience*, *8*(9), 728–733. https://doi.org/10.1038/ngeo2515Austermann, J., Ben-Avraham, Z., Bird, P., Heidbach, O., Schubert, G., & Stock, J. M. (2011). Quantifying the forces needed for the rapid change of Pacific plate motion at 6Ma. *Earth and Planetary Science Letters*, *307*(3–4), 289–297. https://doi.org/10.1016/j.epsl.2011.04.043Baes, M., Govers, R., & Wortel, R. (2011). Switching between alternative responses of the lithosphere to continental collision. *Geophysical Journal International*, *187*(3), 1151–1174. https://doi.org/10.1111/j.1365-246X.2011.05236.xBhattacharya, A., Rekha, S., Sequeira, N., & Chatterjee, A. (2019). Transition from shallow to steep foliation in the Early Neoproterozoic Gangpur accretionary orogen (Eastern India): Mechanics, significance of mid-crustal deformation, and case for subduction polarity reversal? *Lithos*, *348–349*, 105196. https://doi.org/10.1016/j.lithos.2019.105196Brown, D., Herrington, R. J., & Alvarez-Marron, J. (2011). Processes of Arc–Continent Collision in the Uralides. *Springer Berlin Heidelberg*.Chandler, M. T., Wessel, P., Taylor, B., Seton, M., Kim, S. S., & Hyeong, K. (2012). Reconstructing Ontong Java Nui: Implications for Pacific absolute plate motion, hotspot drift and true polar wander. *Earth and Planetary Science Letters*, *331–*

332, 140–151. https://doi.org/10.1016/j.epsl.2012.03.017Covellone, B. M., Savage, B., & Shen, Y. (2015). Seismic wave speed structure of the Ontong Java Plateau. *Earth and Planetary Science Letters*, *420*, 140–150. https://doi.org/10.1016/j.epsl.2015.03.033Crameri, F., Schmeling, H., Golabek, G. J., Duretz, T., Orendt, R., Buiter, S. J. H., et al. (2012). A comparison of numerical surface topography calculations in geodynamic modelling: An evaluation of the "sticky air" method. *Geophysical Journal International*, *189*(1), 38–54. https://doi.org/10.1111/j.1365-246X.2012.05388.xCrameri, Fabio, & Tackley, P. J. (2014). Spontaneous development of arcuate single-sided subduction in global 3-D mantle convection models with a free surface. *Journal of Geophysical Research: Solid Earth*, *119*(7), 5921–5942. https://doi.org/10.1002/2014JB010939Crameri, Fabio, & Tackley, P. J. (2015). Parameters controlling dynamically self-consistent plate tectonics and single-sided subduction in global models of mantle convection. *Journal of Geophysical Research: Solid Earth*, *120*(5), 3680–3706. https://doi.org/10.1002/2014JB011664Crameri, Fabio, Magni, V., Domeier, M., Shephard, G. E., Chotalia, K., Cooper, G., et al. (2020). A transdisciplinary and community-driven database to unravel subduction zone initiation. *Nature Communications*, *11*(1), 3750. https://doi.org/10.1038/s41467-020-17522-9Dai, L., Wang, L., Lou, D., Li, Z., Dong, H., Ma, F., et al. (2020). Slab Rollback Versus Delamination: Contrasting Fates of Flat-Slab Subduction and Implications for South China Evolution in the Mesozoic. *Journal of Geophysical Research: Solid Earth*, *125*(4), 1–18. https://doi.org/10.1029/2019jb019164Duretz, T., Agard, P., Yamato, P., Ducassou, C., Burov, E. B., & Gerya, T. V. (2016). Thermo-mechanical modeling of the obduction process based on the Oman Ophiolite case. *Gondwana Research*, *32*, 1–10. https://doi.org/10.1016/j.gr.2015.02.002Dziewonski, A. M., Chou, T. A., & Woodhouse, J. H. (1981). Determination of earthquake source parameters from waveform data for studies of global and regional seismicity. *Journal of Geophysical Research*, *86*(B4), 2825–2852. https://doi.org/10.1029/JB086iB04p02825Faccenda, M., Gerya, T. V., & Chakraborty, S. (2008). Styles of post-subduction collisional orogeny: Influence of convergence velocity, crustal rheology and radiogenic heat production. *Lithos*, *103*(1–2), 257–287. https://doi.org/10.1016/j.lithos.2007.09.009Falvey, & D. (1975). Part 2. Younger Pacifics arcs and the eastern marginal seas: Arc reversals, and a tectonic model for the North Fiji Basin. *Exploration Geophysics*, *6*(3), 47.Gerya, T. V., Stern, R. J., Baes, M., Sobolev, S. V., & Whattam, S. A. (2015). Plate tectonics on the Earth triggered by plume-induced subduction initiation. *Nature*, *527*(7577), 221–225. https://doi.org/10.1038/nature15752Gerya, T. V., Bercovici, D., & Becker, T. W. (2021). Dynamic slab segmentation due to brittle–ductile damage in the outer rise. *Nature*, *599*(7884), 245–250. https://doi.org/10.1038/s41586-021-03937-xGerya, Taras V., & Yuen, D. A. (2003). Characteristics-based marker-in-cell method with conservative finite-differences schemes for modeling geological flows with strongly variable transport properties. *Physics of the Earth and Planetary Interiors*, *140*(4), 293–318. https://doi.org/10.1016/j.pepi.2003.09.006Guilmette, C.,

Smit, M. A., van Hinsbergen, D. J. J., Gürer, D., Corfu, F., Charette, B., et al. (2018). Forced subduction initiation recorded in the sole and crust of the Semail Ophiolite of Oman. *Nature Geoscience*, *11*(9), 688–695. https://doi.org/10.1038/s41561-018-0209-2von Hagke, C., Philippon, M., Avouac, J.-P., & Gurnis, M. (2016). Origin and time evolution of subduction polarity reversal from plate kinematics of Southeast Asia. *Geology*, *44*(8), 659–662. https://doi.org/10.1130/G37821.1Hall, R. (2002). Cenozoic geological and plate tectonic evolution of SE Asia and the SW Pacific: Computer-based reconstructions, model and animations. *J. Asian Earth Sci.*, *20*. https://doi.org/10.1016/S1367-9120(01)00069-4Van Hinsbergen, D. J. J., Peters, K., Maffione, M., Spakman, W., Guilmette, C., Thieulot, C., et al. (2015). Dynamics of intraoceanic subduction initiation: 2. suprasubduction zone ophiolite formation and metamorphic sole exhumation in context of absolute plate motions. *Geochemistry, Geophysics, Geosystems*, *16*(6). https://doi.org/10.1002/2015GC005745Holm, R. J., Rosenbaum, G., & Richards, S. W. (2016). Post 8 Ma reconstruction of Papua New Guinea and Solomon Islands: Microplate tectonics in a convergent plate boundary setting. *Earth-Science Reviews*, *156*, 66–81. https://doi.org/10.1016/j.earscirev.2016.03.005Holm, R. J., Tapster, S., Jelsma, H. A., Rosenbaum, G., & Mark, D. F. (2019). Tectonic evolution and copper-gold metallogenesis of the Papua New Guinea and Solomon Islands region. *Ore Geology Reviews*, *104*(October 2017), 208–226. https://doi.org/10.1016/j.oregeorev.2018.11.007Hosseini, K, & Sigloch, K. (2015). Multifrequency measurements of core-diffracted P waves (Pdiff) for global waveform tomography. *GEOPHYSICAL JOURNAL INTERNATIONAL*, *203*(1), 506–521. https://doi.org/10.1093/gji/ggv298Hosseini, Kasra, Matthews, K. J., Sigloch, K., Shephard, G. E., Domeier, M., & Tsekhmistrenko, M. (2018). SubMachine: Web-Based Tools for Exploring Seismic Tomography and Other Models of Earth's Deep Interior. *Geochemistry, Geophysics, Geosystems*, *19*(5), 1464–1483. https://doi.org/https://doi.org/10.1029/2018GC007431Huangfu, P., Li, Z. H., Gerya, T., Fan, W., Zhang, K. J., Zhang, H., & Shi, Y. (2018). Multiterrane structure controls the contrasting lithospheric evolution beneath the western and central–eastern Tibetan plateau. *Nature Communications*, *9*(1), 1–11. https://doi.org/10.1038/s41467-018-06233-xIshikawa, A., Maruyama, S., & Komiya, T. (2004). Layered lithospheric mantle beneath the Ontong Java Plateau: Implications from xenoliths in Alnöite, Malaita, Solomon Islands. *Journal of Petrology*, *45*(10), 2011–2044. https://doi.org/10.1093/petrology/egh046Ishikawa, A., Pearson, D. G., & Dale, C. W. (2011). Ancient Os isotope signatures from the Ontong Java Plateau lithosphere : Tracing lithospheric accretion history. *Earth and Planetary Science Letters*, *301*(1–2), 159–170. https://doi.org/10.1016/j.epsl.2010.10.034Isse, T., Suetsugu, D., Ishikawa, A., Shiobara, H., Sugioka, H., Ito, A., et al. (2021). Seismic evidence for a thermochemical mantle plume underplating the lithosphere of the Ontong Java Plateau. *Communications Earth & Environment*, *2*(1), 1–7. https://doi.org/10.1038/s43247-021-00169-

9Jadamec, M. A. (2016). Insights on slab-driven mantle flow from advances in three-dimensional modelling. *Journal of Geodynamics*, *100*, 51–70. https://doi.org/10.1016/j.jog.2016.07.004Knesel, K. M., Cohen, B. E., Vasconcelos, P. M., & Thiede, D. S. (2008). Rapid change in drift of the Australian plate records collision with Ontong Java plateau. *Nature*, *454*(7205), 754–757. https://doi.org/10.1038/nature07138Korenaga, J. (2005). Why did not the Ontong Java Plateau form subaerially? *Earth and Planetary Science Letters*, *234*(3–4), 385–399. https://doi.org/10.1016/j.epsl.2005.03.011Ku, C. S., Kuo, Y. T., Huang, B. S., Chen, Y. G., & Wu, Y. M. (2020). Seismic velocity structure beneath the Western Solomon Islands from the joint inversion of receiver functions and surface-wave dispersion curves. *Journal of Asian Earth Sciences*, *195*(1), 104378. https://doi.org/10.1016/j.jseaes.2020.104378Lallemand, S., & Arcay, D. (2021a). Subduction initiation from the earliest stages to self-sustained subduction: Insights from the analysis of 70 Cenozoic sites. *Earth-Science Reviews*, *221*, 103779. https://doi.org/10.1016/J.EARSCIREV.2021.103779Lallemand, S., & Arcay, D. (2021b). Subduction initiation from the earliest stages to self-sustained subduction: Insights from the analysis of 70 Cenozoic sites. *Earth-Science Reviews*, *221*, 103779. https://doi.org/10.1016/J.EARSCIREV.2021.103779Laske, G., Masters, G., Ma, Z., & Pasyanos, M. (2013). Update on CRUST1.0 - A 1-degree global model of Earth's crust. *Abstract EGU2013-2658 presented at 2013 Geophys. Res. Abstracts 15*, *15*, 2658-.Levin, V., Park, J., Brandon, M., Lees, J., & Ozerov, A. (2002). Crust and upper mantle of Kamchatka from teleseismic receiver functions. *Tectonophysics*, *358*(1), 233–265.Li, C., Van Der Hilst, R. D., Engdahl, E. R., & Burdick, S. (2008). A new global model for P wave speed variations in Earth's mantle. *Geochemistry, Geophysics, Geosystems*, *9*(5). https://doi.org/10.1029/2007GC001806Li, S., Zhao, S., Liu, X., Cao, H., Yu, S., Li, X., et al. (2018). Closure of the Proto-Tethys Ocean and Early Paleozoic amalgamation of microcontinental blocks in East Asia. *Earth-Science Reviews*, *186*, 37–75. https://doi.org/10.1016/J.EARSCIREV.2017.01.011Li, Z. H., Gerya, T., & Connolly, J. A. D. (2019). Variability of subducting slab morphologies in the mantle transition zone: Insight from petrological-thermomechanical modeling. *Earth-Science Reviews*, *196*(March), 102874. https://doi.org/10.1016/j.earscirev.2019.05.018Liu, Z., Dai, L., Li, S., Wang, L., Xing, H., Liu, Y., et al. (2021). When plateau meets subduction zone: A review of numerical models. *Earth-Science Reviews*, *215*(238), 103556. https://doi.org/10.1016/j.earscirev.2021.103556Maffione, M., Thieulot, C., van Hinsbergen, D. J. J., Morris, A., Plümper, O., & Spakman, W. (2015). Dynamics of intraoceanic subduction initiation: 1. Oceanic detachment fault inversion and the formation of supra-subduction zone ophiolites. *Geochemistry, Geophysics, Geosystems*, *16*(6). https://doi.org/10.1002/2015GC005746Maffione, M., van Hinsbergen, D. J. J., de Gelder, G. I. N. O., van der Goes, F. C., & Morris, A. (2017). Kinematics of Late Cretaceous subduction initiation in the Neo-Tethys Ocean reconstructed from ophiolites of Turkey, Cyprus, and Syria. *Journal of Geophysical Research: Solid Earth*, *122*(5), 3953–3976. https://doi.org/10.1002/2016JB013821Mann, P, & Taira, A. (2004). Global tectonic significance of the Solomon Islands and Ontong Java Plateau convergent

zone. *Tectonophysics*, *389*. https://doi.org/10.1016/j.tecto.2003.10.024Mann, Paul, & Taira, A. (2004). Global tectonic significance of the Solomon Islands and Ontong Java Plateau convergent zone. *Tectonophysics*, *389*(3-4 SPEC.ISS.), 137–190. https://doi.org/10.1016/j.tecto.2003.10.024Maunder, B., Prytulak, J., Goes, S., & Reagan, M. (2020). Rapid subduction initiation and magmatism in the Western Pacific driven by internal vertical forces. *Nature Communications*, *11*(1), 1–8. https://doi.org/10.1038/s41467-020-15737-4Müller, R. D., Zahirovic, S., Williams, S. E., Cannon, J., Seton, M., Bower, D. J., et al. (2019). A Global Plate Model Including Lithospheric Deformation Along Major Rifts and Orogens Since the Triassic. *Tectonics*, *38*(6), 1884–1907. https://doi.org/10.1029/2018TC005462Nettles, M., & Dziewon, A. M. (2012). The global CMT project 2004 – 2010 : Centroid-moment tensors, *201*, 1–9.Niu, Y. (2016). Testing the geologically testable hypothesis on subduction initiation. *Science Bulletin*, *61*(16), 1231–1235. https://doi.org/10.1007/s11434-016-1144-5Pasyanos, M. E., Masters, T. G., Laske, G., & Ma, Z. (2014). LITHO1.0: An updated crust and lithospheric model of the Earth. *Journal of Geophysical Research: Solid Earth*, *119*(3), 2153–2173. https://doi.org/https://doi.org/10.1002/2013JB010626Petterson, M. G., Babbs, T., Neal, C. R., Mahoney, J. J., Saunders, A. D., Duncan, R. A., et al. (1999). Geological-tectonic framework of Solomon Islands, SW Pacific: Crustal accretion and growth within an intra-oceanic setting. *Tectonophysics*, *301*(1–2), 35–60. https://doi.org/10.1016/S0040-1951(98)00214-5Plunder, A., Bandyopadhyay, D., Ganerød, M., Advokaat, E. L., Ghosh, B., Bandopadhyay, P., & Hinsbergen, D. J. J. (2020). History of subduction polarity reversal during arc-continent collision: constraints from the Andaman Ophiolite and its metamorphic sole. *Tectonics*, 0–3. https://doi.org/10.1029/2019tc005762Schellart, W. P., Lister, G. S., & Toy, V. G. (2006). A Late Cretaceous and Cenozoic reconstruction of the Southwest Pacific region: Tectonics controlled by subduction and slab rollback processes. *Earth-Science Reviews*, *76*(3–4), 191–233. https://doi.org/10.1016/j.earscirev.2006.01.002Shi, Y. N., Niu, F., Li, Z. H., & Huangfu, P. (2020). Craton destruction links to the interaction between subduction and mid-lithospheric discontinuity: Implications for the eastern North China Craton. *Gondwana Research*, *83*, 49–62. https://doi.org/10.1016/j.gr.2020.01.016Smart, K. A., Tappe, S., Ishikawa, A., Pfänder, J. A., & Stracke, A. (2019). K-rich hydrous mantle lithosphere beneath the Ontong Java Plateau: Significance for the genesis of oceanic basalts and Archean continents. *Geochimica et Cosmochimica Acta*, *248*, 311–342. https://doi.org/10.1016/j.gca.2019.01.013Stern, R. J. (2004). Subduction initiation: Spontaneous and induced. *Earth and Planetary Science Letters*, *226*(3–4), 275–292. https://doi.org/10.1016/j.epsl.2004.08.007Stern, R. J., & Gerya, T. (2018). Subduction initiation in nature and models: A review. *Tectonophysics*, *746*(October 2017), 173–198. https://doi.org/10.1016/j.tecto.2017.10.014Sun, B., Kaus, B. J. P., Yang, J., Lu, G., Wang, X., Wang, K., & Zhao, L. (2021). Subduction Polarity Reversal Triggered by Oceanic Plateau Accretion: Implications for Induced Subduction Initiation. *Geophysical Research Letters*, *n/a*(n/a), e2021GL095299. https://doi.org/https://doi.org/10.1029/2021GL095299Sun,

B., Kaus, B. J. P., Yang, J., Lu, G., Wang, X., Wang, K., & Zhao, L. (2022). Subduction Polarity Reversal Triggered by Oceanic Plateau Accretion: Implications for Induced Subduction Initiation. *Geophysical Research Letters*, *n/a*(n/a), e2021GL095299. https://doi.org/https://doi.org/10.1029/2021GL095299Sutherland, R., Dickens, G. R., Blum, P., Agnini, C., Alegret, L., Asatryan, G., et al. (2020). Continental-scale geographic change across zealandia during paleogene subduction initiation. *Geology*, *48*(5), 419–424. https://doi.org/10.1130/G47008.1Taira, A., Mann, P., & Rahardiawan, R. (2004). Incipient subduction of the Ontong Java Plateau along the North Solomon trench. *Tectonophysics*, *389*(3-4 SPEC.ISS.), 247–266. https://doi.org/10.1016/j.tecto.2004.07.052Tao, J., Dai, L., Lou, D., Li, Z. H., Zhou, S., Liu, Z., et al. (2020). Accretion of oceanic plateaus at continental margins: Numerical modeling. *Gondwana Research*, *81*, 390–402. https://doi.org/10.1016/j.gr.2019.11.015Tapster, S., Roberts, N. M. W., Petterson, M. G., Saunders, A. D., & Naden, J. (2014). From continent to intra-oceanic arc: Zircon xenocrysts record the crustal evolution of the Solomon island arc. *Geology*, *42*(12), 1087–1090. https://doi.org/10.1130/G36033.1Tetreault, J. L., & Buiter, S. J. H. (2012). Geodynamic models of terrane accretion: Testing the fate of island arcs, oceanic plateaus, and continental fragments in subduction zones. *Journal of Geophysical Research: Solid Earth*, *117*(8), 1–23. https://doi.org/10.1029/2012JB009316Tharimena, S., Rychert, C. A., & Harmon, N. (2016). Seismic imaging of a mid-lithospheric discontinuity beneath Ontong Java Plateau. *Earth and Planetary Science Letters*, *450*, 62–70. https://doi.org/10.1016/j.epsl.2016.06.026Turcotte, D. L., & Schubert, G. (2002). *Geodynamics* (2nd ed). Cambridge: Cambridge University Press. https://doi.org/DOI: 10.1017/CBO9780511807442Vaes, B., Van Hinsbergen, D. J. J., & Boschman, L. M. (2019). Reconstruction of Subduction and Back-Arc Spreading in the NW Pacific and Aleutian Basin: Clues to Causes of Cretaceous and Eocene Plate Reorganizations. *Tectonics*, *38*(3–4), 1367–1413.Vogt, K., & Gerya, T. (2014). Deep plate serpentinization triggers skinning of subducting slabs. *Geology*, *42*(8), 723–726. https://doi.org/10.1130/G35565.1Xu, Z. Q., Yang, J., Li, W. C., Li, H. Q., Cai, Z., Yan, Z., & Ma, C. (2013). Pako-Tethys system and accretionary orogen in the Tibet Plateau. *Acta Petrologica Sinica*, *29*, 1847–1860.Zhang, S., & Leng, W. (2021). Subduction Polarity Reversal: Induced or Spontaneous? *Geophysical Research Letters*, *48*(11), e2021GL093201. https://doi.org/10.1029/2021GL093201Zhou, X., & Wada, I. (2021). Differentiating induced versus spontaneous subduction initiation using thermomechanical models and metamorphic soles. *Nature Communications*, *12*(1), 1–10. https://doi.org/10.1038/s41467-021-24896-xZhou, X., Li, Z. H., Gerya, T. V., Stern, R. J., Xu, Z., & Zhang, J. (2018). Subduction initiation dynamics along a transform fault control trench curvature and ophiolite ages. *Geology*, *46*(7), 607–610. https://doi.org/10.1130/G40154.1Zhou, X., Li, Z. H., Gerya, T. V., & Stern, R. J. (2020). Lateral propagation-induced subduction initiation at passive continental margins controlled by preexisting lithospheric weakness. *Science Advances*, *6*(10), 1–10. https://doi.org/10.1126/sciadv.aaz1048

Figure caption

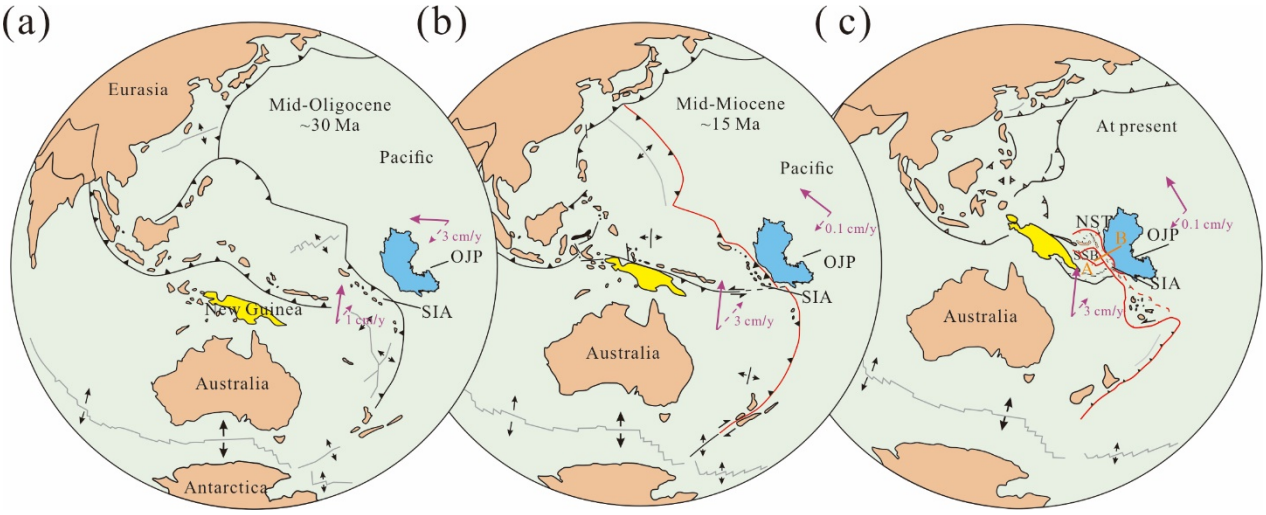

Figure 1 Simplified reconstruction of the western Pacific Ocean. Tectonic reconstruction of the western Pacific Ocean during (a) Mid-Oligocene (~30 Ma), (b) Mid-Miocene (~15 Ma), and (c) Early-Pliocene (At present), according to a previous dataset (Mann & Taira, 2004; Knesel et al., 2008). The light blue area represents the Ontong Java Plateau (OJP), the red lines are plate boundaries, the purple arrows indicate the general direction of plate motion, the purple dashed arrows indicate the velocity components in the general direction of OJP-SIA, and the line (A-B) represents the sampling points of Figure 2. SSB-Solomon Sea Basin; SIA-Solomon Island Arc; OJP-Ontong Java Plateau. NST-North Solomon Trench.

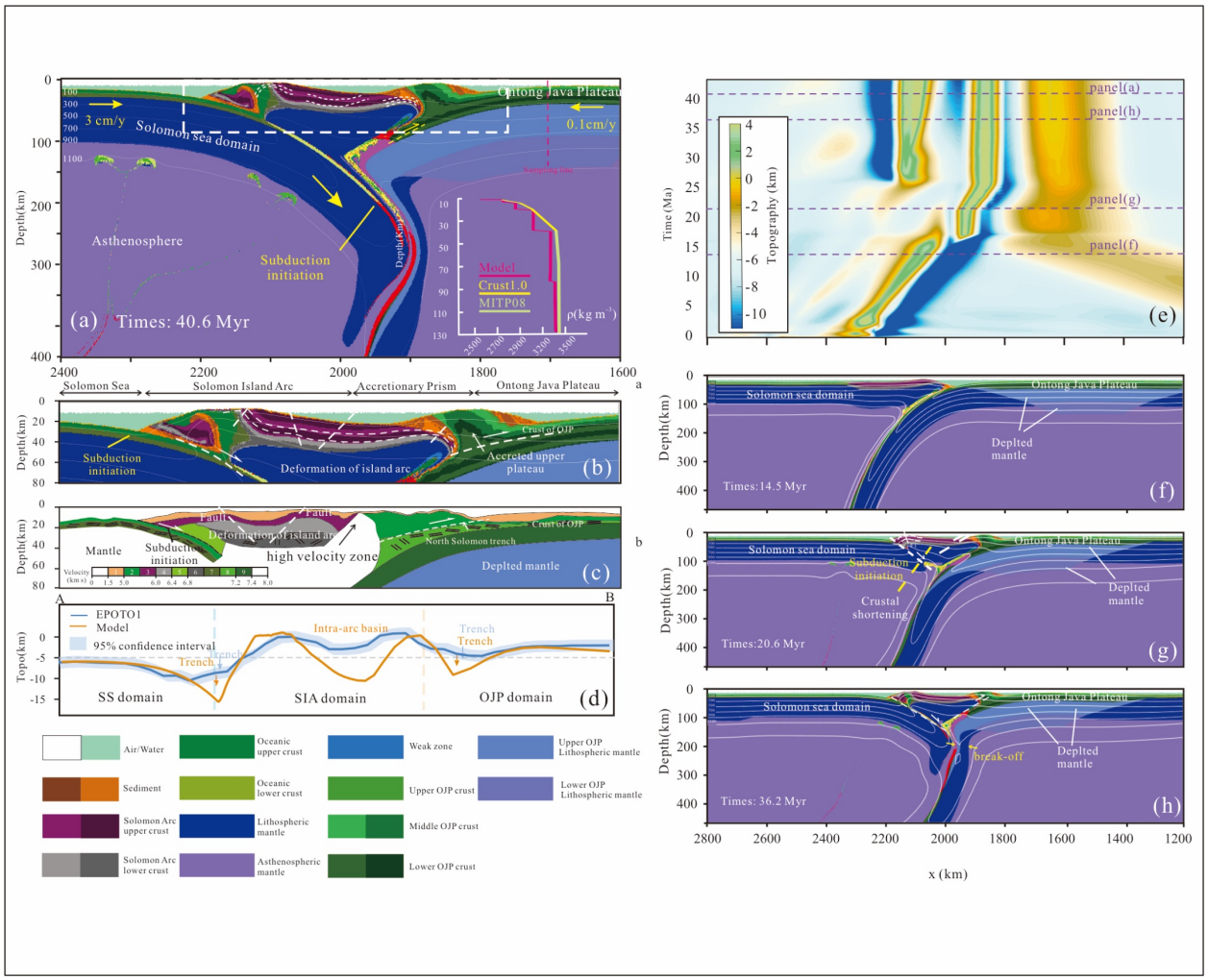

Figure 2 Evolution of the reference model and comparison with real data (a) The reference model triggered by a large-scale oceanic plateau (after 40.6 Myr in the experiment). Modeled density profiles (red line) and the density profiles from the Crust1.0 (yellow lines) (Jadamec, 2016) and the density profiles from the MITP08 (the light yellow) (Li et al., 2008) of the OJP are shown as the inset in **(a)**. The color key for different materials is shown at the bottom.**(b)** Deformation of model in the white dashed box in panel (a). **(c)** The major geologic provinces of the SIA based on P-wave velocity (modified from Mann et al., 2004). The lower left figure represents the specific wave speed range. **(d)** Topographic profile of the reference model (thick orange line) and the observations (thick blue line). The sampling points are shown by orange lines in Figure. 1c.**(e)** Topographic evolution of the model. The color bar is shown in inset. **(f-g)** Evolution of the reference model.

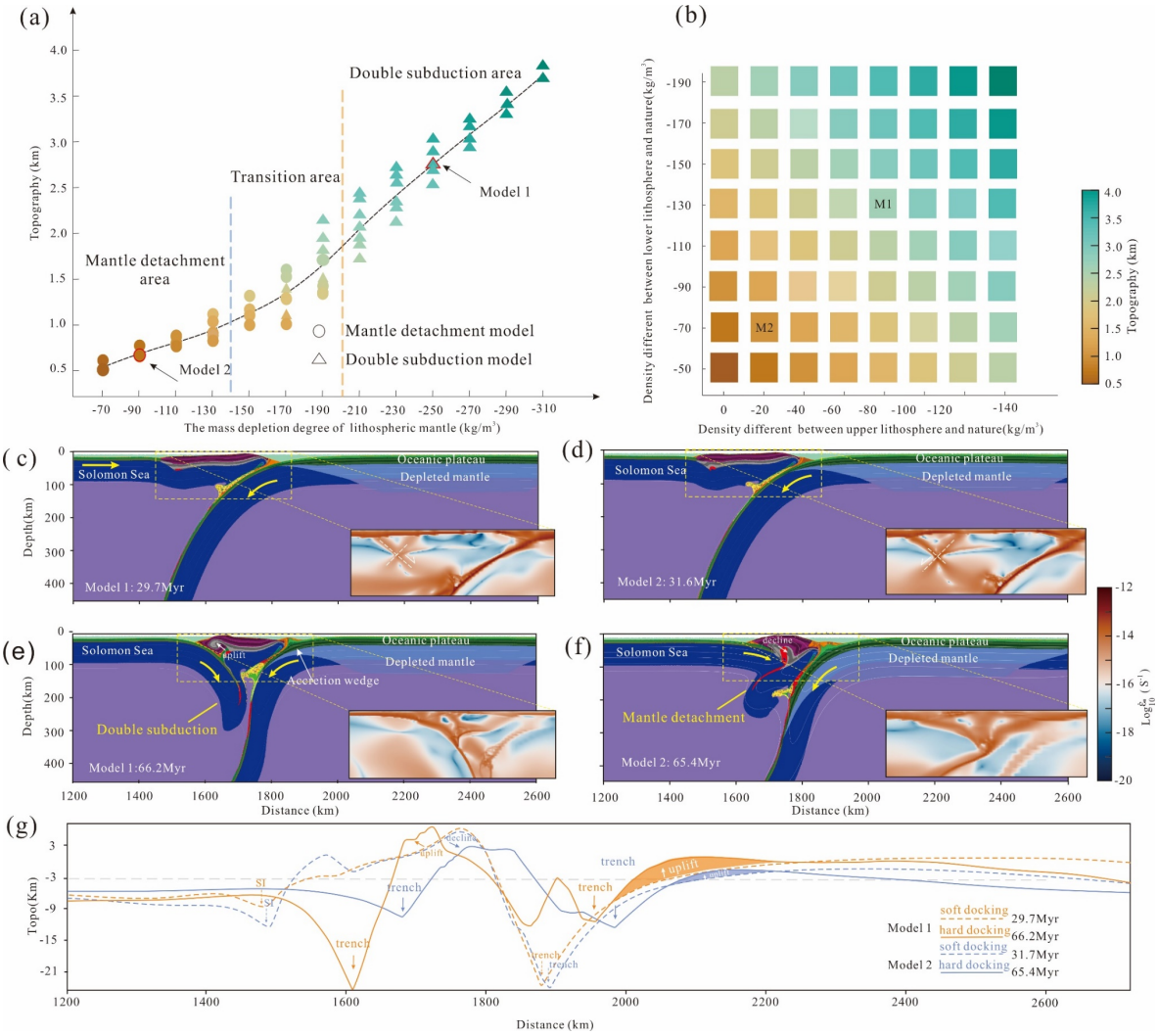

Figure 3 Summary of model results with varying degree of depletion in the lithospheric mantle of the oceanic plateau. **(a)** The average topography uplift caused by the OJP mantle depletion. The locations of the sampling line are shown in Figure S1. Circles represent models that developed mantle detachments and triangles represent models that developed double subduction zones. The colors represent the average terrain height and the color bar is shown in the right upper side of figure. Topographic uplift is relative to the initial seafloor level (17 km). **(b)** Phase diagram with variable depletion degrees of the upper and lower parts of the lithospheric mantle. Note, the density variation in the lithospheric mantle is relative to the normal density (3300 kg/m^3). **(c-f)** The evolution of Model 1 (the double subduction model after **(c** 29.7 Myr, **(e)** 66.2 Myr) and the Model 2 (the mantle detachment model after

(d) 31.6 Myr, **(f)** 65.4 Myr) have elapsed. The inset in the lower right of each panel represents the second invariant of strain rate. The color bar of strain rate is shown in the right side of Figure **(g)** Four topographical cross-sections corresponding to the four time periods shown in panels **(c-f)**. The orange lines represent topography results from Model 1 (the double subduction model in **(c-e)**), and the blue lines represent topography results from Model 3 (the mantle detachment model in **(d-f)**). The orange and blue areas represent plateau uplift in Models 1 and 2, respectively. This series of models has an island arc length of 350 km, an island arc thickness of 28 km in right and 34 km in left, lithospheric thickness of back-arc basin of 88 km.

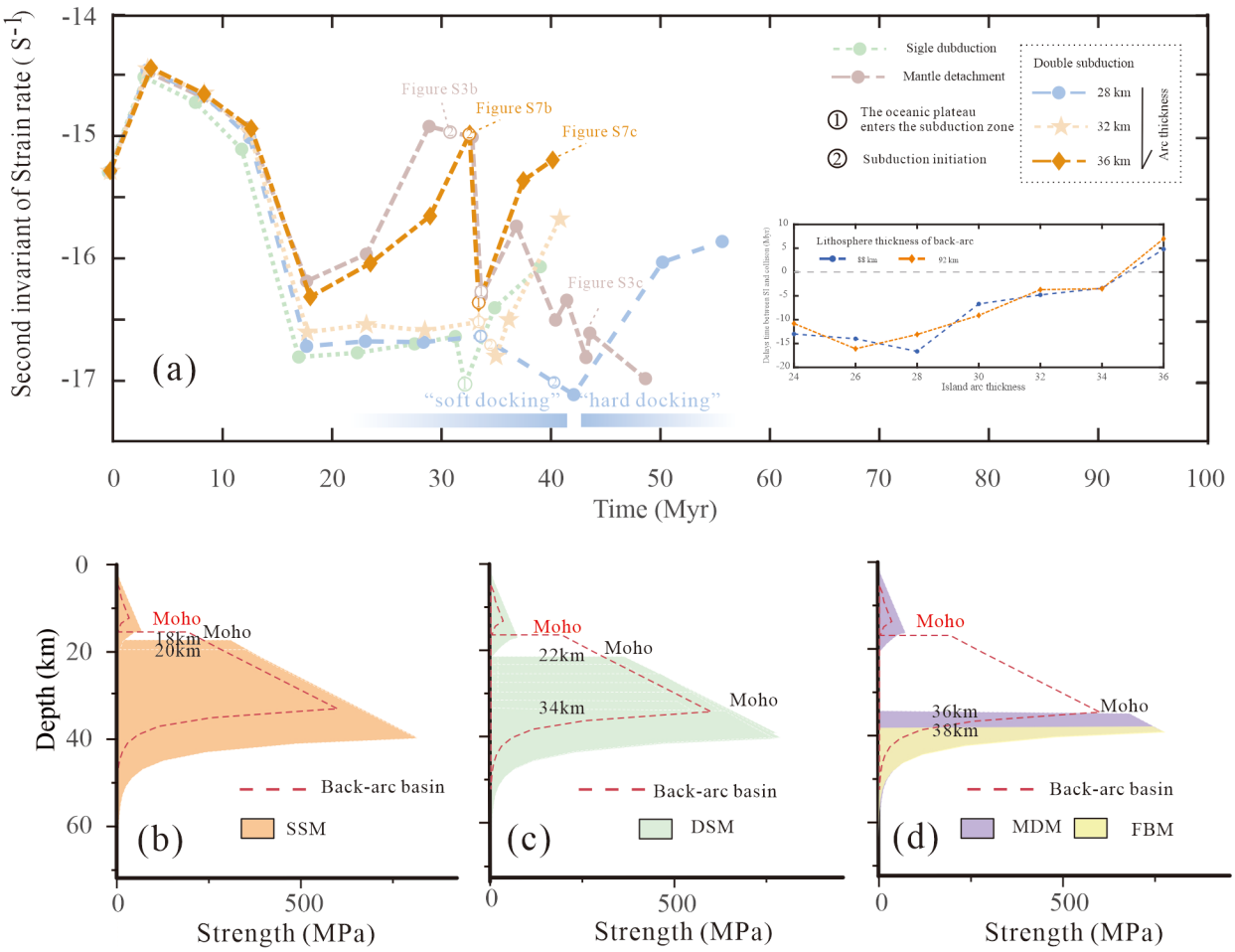

Figure 4 Evolution of the second invariance of strain rate at the intersection of island arc and retro-arc basin and 1D strength profiles from the initial lithological sequence of the arc show the representative distribution of differential stress with island arc thickness. (a)

The evolution of the second invariance of strain rate at the intersection of island arc and back-arc basin for different models, i.e. the single subduction (light green line), the mantle detachment (brown line), the double subduction (blue line (island arc thickness 28km), light orange line (island arc thickness 30km), orange line (island arc thickness 32km)). The inset diagram is correlation of SI and plateau collision time delays with island arc thickness. The colors represent the different lithospheric thickness of back-arc, i.e. 88 km (blue line) and 92 km (orange line). **(b-d)** 1D strength profiles from the initial lithological sequence of the arc show the representative distribution of differential stress with island arc thickness. The red dotted line represents the strength of the back-arc basin. This series of models can be found in Figure S2 which has an island arc length of 350 km and lithospheric thickness of back-arc basin of 88 km. The orange, light green, purple and yellow areas represent the SSM,DSM, MDM, and FBM model lithospheric responses, respectively. DSM-Double subduction zone, SSM-Single subduction zone, MDM-Mantle detachment, and FBM-Fractured basin subduction.